RSC Advances

PAPER

View Article Online
View Journal | View Issue

Cite this: *RSC Adv.*, 2015, **5**, 105416

Antibacterial surfaces based on functionally graded photocatalytic Fe_3O_4@TiO_2 core–shell nanoparticle/epoxy composites

Tommaso Nardi,[a] Sami Rtimi,*[b] Cesar Pulgarin[b] and Yves Leterrier*[a]

Received 18th September 2015
Accepted 30th November 2015

DOI: 10.1039/c5ra19298f

www.rsc.org/advances

Functionally graded epoxy composites with various concentration profiles of Fe_3O_4@TiO_2 core–shell nanoparticles (NPs) were synthetized and characterized, with focus on their antibacterial properties. The NPs consisted of rutile, anatase, magnetite and hematite. Graded composites were produced starting with homogeneous 2 vol% to 12 vol% NPs suspensions using a magnetophorese process, leading to an enrichment of TiO_2 at the surface of the composite up to 16 vol% from an initial 4 vol%. Homogeneous composites were also produced as references. Graded composites with an initial 4 vol% of NPs inactivated *E. coli* bacteria in less than 2 hours under simulated solar light (50 mW cm^{-2}), significantly faster than their homogeneous analogues. During bacterial inactivation the pH decreased from 6.8 to 5.0. Repetitive *E. coli* inactivation tests on these 4 vol% graded composites were stable up to 8 cycles and 5 min contact between the bacteria and the sample surface was enough to guarantee an adequate bacterial adhesion.

Introduction

During the last decade a lot of interest has been drawn to develop more efficient self-cleaning/self-sterilizing surfaces and polymers due to the growth of the world population and the increasing number of bacterial infections coming from polymeric fabrics. These self-sterilizing polymer surfaces can provide a protection against bacterial infections under light irradiation due to the production of reactive oxygen species (ROS). Self-sterilization is moreover beneficial for the environment avoiding traditional energy intensive and polluting cleaning processes involving detergents/chemicals and antibiotics. Healthcare associated infections (HCAI) have become more frequent in the last decade.[1,2] Bacteria and other pathogens induce infections leading to hospital-acquired infections (HAI) with its associated high health care costs needing a lot of antibiotics.[3–6] But antibiotics administered for long times lead to the development of bacterial resistance. There is thus a need to develop stable antibacterial materials presenting fast bacterial reduction kinetics, long-term operational lifetime and acceptable biocompatibility.[7–10]

Photocatalysis as a useful tool for the self-sterilizing property of glass, polymer thin films and textile fabric surfaces has recently been reported by Daoud *et al.*,[11] Pulgarin, Kiwi *et al.*,[12–16] Hashimoto *et al.*,[17] Bahnemann *et al.*[18] among many others.[19,20] TiO_2 has been chosen as the standard photocatalyst used in the field of environmental photochemistry due to its stability, effective separation of charges under band-gap irradiation and its low cost. The self-sterilizing ability of TiO_2 modified surfaces is basically a photo-oxidative process requiring light, O_2 (air) and water vapor in the air to produce highly oxidative radicals able to destroy organic compounds and/or bacteria.[9,10]

Iron oxide particles can be manipulated using magnetic field gradients.[21–23] Magnetic nanoparticles have been investigated due to their potential use in catalysis, Fenton/Photo-Fenton processes for water treatment[24] including nanomaterial-based catalysts,[25] biomedicine and biomedical applications.[26,27] Core–shell nanoparticles with superparamagnetic iron oxide cores have been synthesized for photocatalytic applications.[28]

In this study we investigated the synthesis, morphology and antibacterial activity of homogeneous and graded composites based on magnetic/photocatalytic Fe_3O_4@TiO_2 core–shell nanoparticles in an epoxy matrix. Starting with different concentrations of nanoparticles (NPs) suspensions in the liquid epoxy prepolymer and using a magnetophorese process, polymer composite surfaces with controlled concentrations of photocatalytic TiO_2 were produced.

Experimental

Materials

Titanium(IV) chloride (99.9%) was purchased from Acros. Hydrogen peroxide (30%) was purchased from Reactolab SA. The epoxy resin DER 321 was purchased from Dow whereas the hardener diethylenetriamine was purchased from Aldrich.

[a]*Laboratoire de Technologie des Composites et Polymères (LTC), Ecole Polytechnique Fédérale de Lausanne (EPFL), CH-1015 Lausanne, Switzerland. E-mail: yves.leterrier@epfl.ch; Tel: +41 216934848*

[b]*Groupe des Procédés Avancés d'Oxydation (GPAO), Ecole Polytechnique Fédérale de Lausanne (EPFL), CH-1015, Lausanne, Switzerland. E-mail: sami.rtimi@epfl.ch; Tel: +41 216936150*

Ammonia solution (25% min) was purchased from VWR. All products were used as received without any further purification.

Synthesis of Fe_3O_4@TiO_2 core–shell nanoparticles

To synthesize the Fe_3O_4 cores, the Bumb *et al.* procedure was followed.[29] Briefly, 8 mmol of $FeCl_3 \cdot 6H_2O$ and 4 mmol of $FeCl_2 \cdot 4H_2O$ were dissolved in 190 ml deionized water at room temperature and stirred in a beaker. Under vigorous stirring, 10 ml of 25% NH_3 was poured down the vortex into the iron solution. Magnetite precipitated a black precipitate. After stirring for 10 minutes, the particles were centrifuged and dispersed in 50 ml deionized water.

The synthesized Fe_3O_4 nanoparticles were subsequently coated exploiting the following procedure reported by Buscaglia *et al.*[30] First, 0.7 ml of $TiCl_4$ were added to the ice-cooled solution of Fe_3O_4 nanoparticles in water (50 ml). Then, a peroxo–titanium complex was prepared by adding 2.7 ml of H_2O_2 (30%) to the Fe_3O_4/$TiCl_4$ solution. The pH was increased by addition of 10 ml of aqueous ammonia (5.44 mol l^{-1}) and the solution was then slowly heated to 95 °C for 5 h. Finally, the solution was cooled down to room temperature and particles were washed and collected by centrifugation. The synthesized nanoparticles were calcined at 450 °C for 6 hours under N_2 flow (10 ml min^{-1}).

Characterization

X-ray powder diffraction (XRPD) data were collected using a Bragg–Brentano θ–2θ diffractometer (Philips PW 1729 PANalytical, Netherlands). The radiation source was an X-ray tube with copper radiation (λ $CuK_{\alpha 1} = 1.54059$ Å) and the anode tube load was 40 kV and 35 mA. The samples were loaded on a quartz flat holder in order to have a zero background. XRPD patterns were collected at room temperature in the 15–135° 2θ range, with a scanning rate of 0.004° s^{-1} and a step size of 0.02° 2θ. Preliminary qualitative phase analyses were performed using the X'Pert High Score Plus software (PANalytical, Netherlands). In order to determine the amorphous phase content of each powder, pure α-Fe_2O_3 was chosen as internal standard. Mixed samples were prepared diluting original samples with 10 wt% of hematite. The concentration gradients were investigated analyzing the Ti content by scanning electron microscopy with energy dispersive X-ray spectroscopy analysis (SEM-EDX) using a FEI XLF-30 FEG at an accelerating voltage V_{acc} of 13 kV and at a constant working distance (11 mm) and spot size (4). Magnetization loops of Fe_3O_4@TiO_2 core–shell NPs in powder form were measured at $T = 295$ K by means of a Vibrating Sample Magnetometer (VSM) operating in the ± 15 kOe field range and equipped with a liquid N_2 continuous-flow cryostat.

Antibacterial tests

E. coli K12 strains was obtained from the Deutsche Sammlung von Mikroorganismen und Zellkulturen GmbH (DSMZ) ATCC23716, Braunschweig, Germany, to test the antibacterial activity of the samples. The samples were sterilized by keeping them at 60 °C for 2 h prior to the antibacterial test experiment. The 100 μl culture aliquots with an initial concentration of $\sim 10^7$ CFU ml^{-1} in NaCl/KCl (pH 7) were placed on the surface of Fe_3O_4@TiO_2 NPs/epoxy composite samples and of pure epoxy samples (control). Samples were then placed on Petri dishes provided with a lid to prevent evaporation. After each determination, the sample was transferred into a sterile tube containing a volume of 900 μl autoclaved NaCl/KCl saline solution. This solution was subsequently mixed thoroughly using a Vortex for 2 min. Serial dilutions were made in NaCl/KCl solution. A 100 μl aliquot was pipetted onto a nutrient agar plate and then spread over the surface of the plate using standard plate method. Agar plates were incubated lid down, at 37 °C for 24 h before counting the CFU. To verify that no re-growth of *E. coli* occurred after the first bacterial inactivation cycle, the remained 900 μl was incubated for 24 hours at 37 °C. Then, 100 μl from this latter solution was deposited on three Petri dishes to obtain replicates. The samples were incubated at 37 °C for 24 h. No bacterial re-growth was observed for these samples. Three bacterial inactivation assays were made and statistical data were calculated according to the standard deviation at 5%.

The samples were irradiated with the Xe-400 W lamp in the Suntest solar simulator CPS (Atlas GmbH, Hanau, Germany) with a light dose of 50 mW cm^{-2} ($\sim 0.8 \times 10^{16}$ photons per s) and a cut-off filter was added in the Suntest cavity to filter the light <310 nm. Irradiation of the samples was carried out on glass Petri dishes provided with a lid to prevent bacterial suspension evaporation. The micro-oxidation analysis (μpH) followed the changes of pH at the surface of the Fe_3O_4@TiO_2 NPs/epoxy composite contacted with the bacterial suspension. It was followed by means of a pH/mV/Temp meter (Jenco 6230N) equipped with a microprocessor and a RS-232-C IBM interface.

The adhesion of the *E. coli* to the surface of the composite samples was evaluated by immersing the samples into 5 ml *E. coli* suspensions and shaking these gently at 37 °C in the dark to avoid any photocatalytic inactivation effects.[30,32] Non-adhered bacteria were subsequently removed by washing the samples with a phosphate buffer solution (pH 7.2). The number of viable cells was determined after removal of adhered *E. coli* cells by ultrasonication for 15 min (Elgasonic bath, power 50 W).

Results and discussion

Characterization of Fe_3O_4@TiO_2 core–shell nanoparticles

The Rietveld quantitative phase analysis performed on Fe_3O_4@TiO_2 NPs shown in Fig. 1 evidenced how they exhibited a partially crystalline shell, with an anatase content of $\approx$35 wt%. The overall composition of the NPs is reported in Table 1.

The magnetization curve of Fe_3O_4@TiO_2 NPs shown in Fig. 2 is characterized by the absence of magnetic hysteresis and by a saturating behavior at high magnetic fields. In particular, the high-field magnetization resulted to be 11.3 emu g^{-1}.

Graded concentrations of Fe_3O_4@TiO_2 core–shell NPs in epoxy

Suspensions of Fe_3O_4@TiO_2 core–shell NPs in liquid epoxy at selected concentrations (2, 4, 6, and 12 vol%) were subjected to an external magnetic field gradient generated by two permanent magnets in repulsion configuration. In order to minimize the

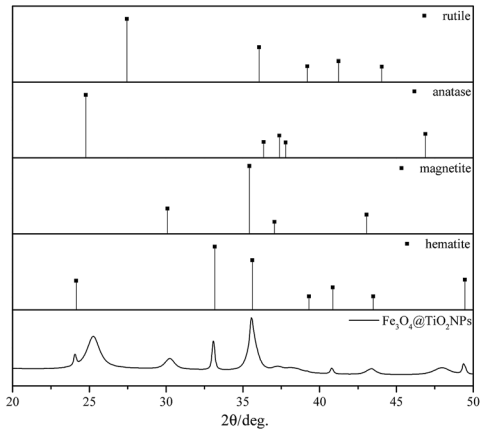

Fig. 1 XRD plots of the Fe_3O_4@TiO_2 nanoparticles and reference lines of rutile, anatase, magnetite and hematite.

Table 1 Quantification of crystalline/amorphous phase in Fe_3O_4@TiO_2 nanoparticles (weight%) as determined by XRD

Particles	Rutile	Anatase	Crystalline magnetite	Amorphous
Fe_3O_4@TiO_2	0	35.18 ± 0.20	32.58 ± 0.23	32.24 ± 0.50

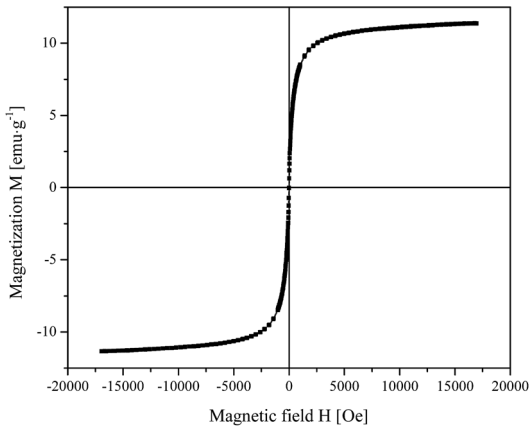

Fig. 2 Room temperature magnetization curve of Fe_3O_4@TiO_2 nanoparticles.

processing time, the curing of the nanocomposites and the application of the magnetic field gradient were carried out simultaneously for 2 h at 60 °C. Fig. 3 shows cylindrical coupons of the pure epoxy, homogeneous and graded composites with different concentrations of NPs. The epoxy was transparent, whereas the homogeneous composites were not, their degree of opacity increasing with NPs concentration. In contrast, the graded composites exhibited a gradient in opacity, the NP rich surface being fully opaque and the opposite surface being more transparent.

The concentration gradients developed during the dual process in the 1.5–2 mm thick composite coupons are reported in Fig. 4. A concentration gradient from 1.5 to 6 vol% developed

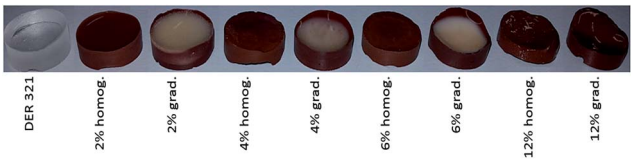

Fig. 3 Cylindrical coupons (diameter 10 mm, thickness ~ 1.5–2 mm) of the pure epoxy (DER 331), homogeneous Fe_3O_4@TiO_2 NPs/epoxy composites (homog.) and graded Fe_3O_4@TiO_2 NPs/epoxy composites (grad.) with different vol% concentrations of NPs as indicated. The graded composites were produced using a magnetophorese process with magnetic field gradient parallel to the axis of the cylindrical coupons oriented towards the bottom of the coupons (NPs-rich surface) on the figure.

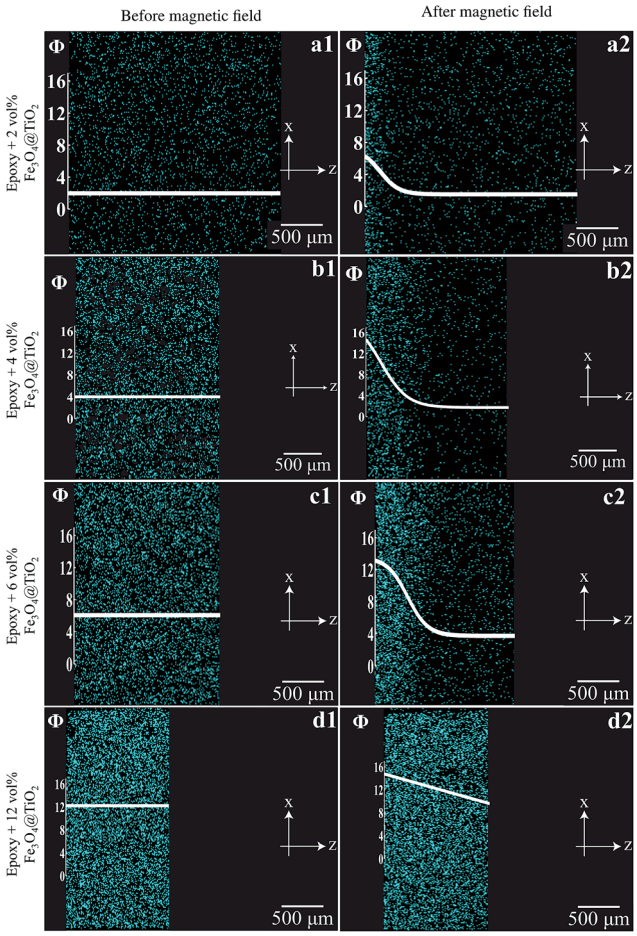

Fig. 4 Cross-sectional SEM-EDX spectral images showing the Ti content (blue) of homogeneous (left column) and graded (right column) composites samples with 2, 4, 6 and 12 vol% of Fe_3O_4@TiO_2 NPs. The superimposed white curves indicate the nanoparticle volume fraction along the sample cross-section.

when the nanocomposite containing an initial concentration of 2 vol% of Fe_3O_4@TiO_2 NPs was subjected to the external magnetic field (Fig. 4a1 and a2). Steeper gradients were achieved when the same magnetic force was applied to suspensions containing 4 vol% and 6 vol% of nanoparticles. In particular, in the former case the gradient spanned the range 2 to 14.5 vol%

(Fig. 4b1 and b2), whereas in the latter case it was from 3.5 to 13 vol% (Fig. 4c1 and c2). A smoother linear gradient ranging from 9 to 15 vol% (Fig. 4d1 and d2) developed when the external magnetic field was applied to a 12 vol% suspension.

The thickness of the central part of the nanocomposites varied as a function of the nanoparticles loading (Fig. 4). In particular, a higher nanoparticle concentration in the polymer led to thinner samples due to the fact that the magnetic force acting on the nanoparticles was not exactly perpendicular to the surface of the magnet. This induced a magnetophorese of the nanoparticles towards the edge of the circular sample and a concurrent motion of the polymer matrix.

Antibacterial activity of homogeneous and graded Fe_3O_4@TiO_2 NPs/epoxy composites

Fig. 5 shows the bacterial inactivation kinetics at the surface of pure epoxy and of homogeneous and graded composites with 2, 4, 6 and 12 vol% of Fe_3O_4@TiO_2 NPs under simulated solar light (50 mW cm^{-2}). It is evident that the pure epoxy had no activity and the homogeneous composite with 6 vol% NPs tested in the dark had a marginal activity. On the opposite, the composites exhibited a clear antibacterial activity with different kinetics depending on the Fe_3O_4@TiO_2 NPs composition. The impact of the Fe_3O_4 cores on the photocatalytic process is negligible since the bandgap of Fe_3O_4 is lower than that of TiO_2, *i.e.*, the oxidative potential of UV-generated Fe_3O_4 holes is insufficient to oxidize water and generate HO radicals. In addition the access of Fe_3O_4 cores by both light and bacteria is limited by the TiO_2 shell.

Homogeneous composites exhibited increasing antibacterial activity with increasing concentration of TiO_2 NPs up to a concentration of 6 vol%, and then decreasing at the highest investigated concentration of 12 vol%. The two faces of the cylindrical samples gave a similar bacterial inactivation potential. Such a decrease at higher concentration was already reported[31] and attributed to the longer inward charge diffusion length of the TiO_2 cb (e^-) and vb (h^+) to reach the surface of the highly loaded composite samples where the photocatalytic interaction with the bacteria takes place.

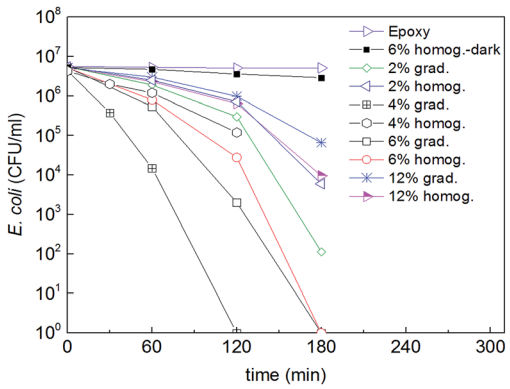

Fig. 5 *E. coli* inactivation kinetics on the surface of pure epoxy, homogeneous (homog.) and graded (grad.) Fe_3O_4@TiO_2 NPs/epoxy composites with 2, 4, 6 and 12 vol% of NPs under simulated solar light (50 mW cm^{-2}).

The optimum NPs concentration was found to be equal to 4 vol% for graded composites, showing the fastest bacterial inactivation kinetics. Concentrations lower and higher than 4 vol% of Fe_3O_4@TiO_2 systematically led to longer bacterial inactivation times. At 4 vol% the concentration of NPs at the surface was 16 vol% (Fig. 5) corresponding to an optimal amount of active sites. This result seems to contradict the inactivation rates of the homogeneous composites, which decreased at surface concentrations above 4 vol%. The surface concentration in the graded composites with 2 vol% of NPs was 6 vol%, lacking enough active sites enabling fast inactivation kinetics. In graded composites with 6 vol% and 12 vol% the surface concentration was 13 vol% and 15 vol%, respectively, and thus should lead to similar behavior compared with the 4 vol%, which was not the case. These apparently contradictory results reflect the complex interplay between two main concentration-dependent phenomena. On one hand, the occurrence of particle clustering at high concentration due to dipolar interactions during the magnetophorese process creates anisotropic structures normal to the surface of the composite, which would decrease the available TiO_2 contact surface with bacteria.[10,32,33] The aspect ratio of these nanoparticulate structures may also favor antibacterial activity.[34] On the other hand, two factors may contribute to the reduced antibacterial activity at high TiO_2 concentration. First is the reduced ROS generation per TiO_2 particle for increased TiO_2 concentration under fixed irradiance (in photons per m^2). Second is the increased recombination or decay of the 'diluted' and short-lived ROS (especially those generated in the internal part of the TiO_2 layers) before they reach the external TiO_2 surface, also for increased TiO_2 concentration, and resulting reduction of bacteria inactivation. The latter TiO_2 bactericide mechanism has been reported elsewhere and will not be discussed in this study.[1,2,24] Work is ongoing to further analyze these results.

The local pH changes on the surface of the graded epoxy composites with 4 vol% of Fe_3O_4@TiO_2 NPs was followed during the bacterial inactivation time and found to decrease stepwise from ~6.8 to ~5.4. This is equivalent to an increase of one and a half orders of magnitude in the proton concentration during bacterial inactivation. This means that H^+ generation predominated over OH^- since a displacement to more acidic pH-values was observed during *E. coli* inactivation. The TiO_2 vb(h^+) oxidized the surface Ti–OH generating OH$^\bullet$-radicals due to the water chemisorbed on the TiO_2 leading to the hole transfer.[35]

One of the challenges for antibacterial surfaces is the stability and the long operational time. This is why we investigated the bacterial inactivation stability during several cycles. Fig. 6 shows that the surface of Fe_3O_4@TiO_2 NPs embedded in epoxy resin led to repetitive bacterial inactivation up to 8 cycles. After each cycle samples were kept in the dark to eliminate any residual photocatalytic ROS-species that may still reactivate on the catalyst surface. The chemical state of the Fe_3O_4@TiO_2 NPs embedded in epoxy resin surface remained stable after the

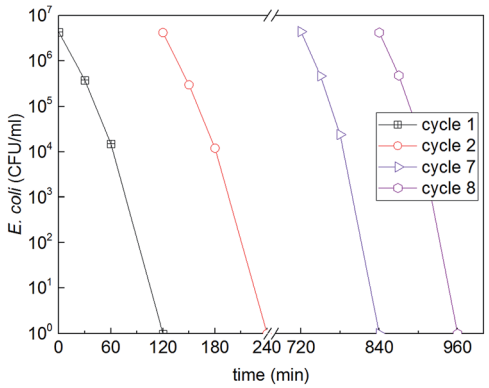

Fig. 6 Cyclic *E. coli* inactivation on the surface of a graded composite with 4 vol% of Fe_3O_4@TiO_2 NPs in epoxy under simulated solar light (50 mW cm^{-2}).

bacterial inactivation cycles. This means that the active sites on the surface remained active to kill adhered bacteria on the surface.

Bacterial adhesion to the surface of the homogeneous and graded epoxy composites with 4 vol% of Fe_3O_4@TiO_2 NPs was also investigated. Fig. 7 shows that 5 min contact between bacteria and the composite surface was enough to guarantee an adequate bacterial adhesion. Longer contact times did not further increase the bacterial loading on the sample surface. For a 1 cm diameter sample (surface 0.79 cm^2), 10^6 to 10^7 *E. coli* can be adsorbed on the surface, since *E. coli* is ~1 μm^2. In fact the prepared surface microstructure was rather rough and not all the inoculated bacteria adsorbed on the surface. Our results nevertheless show that: (a) 5 min of adsorption was necessary to permit bacteria to reach and be adsorbed on the sample surface, and (b) increasing the concentration of NPs led to high surface roughness, reducing bacterial adhesion as recently reported.[31] The bacterial adhesion on the graded composite with 4 vol% of Fe_3O_4@TiO_2 NPs was systematically higher than that on the homogeneous analogue, which was consistent with the higher density of active/polar sites and resulting electrostatic interactions with bacteria.

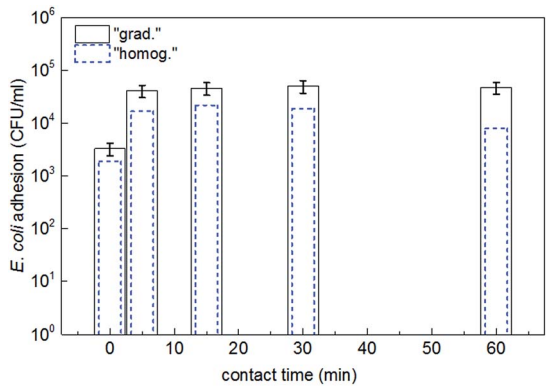

Fig. 7 *E. coli* adhesion on the surface of homogeneous and graded epoxy composites with 4 vol% of Fe_3O_4@TiO_2 NPs as a function of contact time between bacteria and the surface.

Conclusions

Homogeneous and graded epoxy composites with different concentration profiles of Fe_3O_4@TiO_2 NPs were synthesized, using a magnetophorese process for the graded materials, and their antibacterial activity was characterized. The composite surfaces showed effective antibacterial performance with inactivation in less than few hours. The fastest bacterial inactivation was observed for graded composites with a surface concentration of 16 vol% of Fe_3O_4@TiO_2 NPs based on an initial concentration of 4 vol%. This was attributed to the suitable amount of NPs and their anisotropic distribution in the subsurface layers facing the bacteria. This graded material also led to a stable repetitive bacterial inactivation up to 8 cycles. Such graded polymer composite surfaces produced using cost-effective process techniques can be of potential use in hospitals, schools and public places reducing infections.

Acknowledgements

We thank the EPFL and the Swiss National Science Foundation (SNF Projects 200020-155888/1 and 200021-143283/1) for financial support of this work.

References

1 S. Rtimi, C. Pulgarin, R. Sanjines and J. Kiwi, *RSC Adv.*, 2013, **3**, 16345.
2 S. Rtimi, R. Sanjines, M. Andrzejczuk, C. Pulgarin, A. Kulik and J. Kiwi, *Surf. Coat. Technol.*, 2014, **254**, 333.
3 B. Allegranzi, S. Bagheri-Nejad, C. Combescure, W. Graafmans, H. Attar, L. Donaldson and D. Pittet, *Lancet*, 2011, **337**, 228.
4 R. Plowman, R. Graves, N. Griffin and L. Taylor, *J. Hosp. Infect.*, 2001, **47**, 198.
5 S. Dance, *J. Hosp. Infect.*, 2007, **7**, 378.
6 I. Kramer, I. Schwebke and G. Kampf, *BMC Infect. Dis.*, 2006, **6**, 137.
7 S. Rtimi, O. Baghriche, R. Sanjines, C. Pulgarin, M. Bensimon and J. Kiwi, *J. Photochem. Photobiol., A*, 2013, **256**, 52.
8 A. Fujishima, K. Hashimoto and T. Watanabe, *TiO_2 Photocatalysis, Fundamental and Applications*, BCK, Tokyo, 2000.
9 A. Fujishima, X. Zhang and D. Tryck, *Surf. Sci. Rep.*, 2008, **63**, 515.
10 J. Schneider, M. Matsuoka, M. Takeuchi, J. Zhang, Y. Horiuchi, M. Anpo and D. Bahnemann, *Chem. Rev.*, 2014, **114**, 9919.
11 S. Afzai, W. Daoud and S. Langford, *ACS Appl. Mater. Interfaces*, 2013, **11**, 4753.
12 J. Kiwi and C. Pulgarin, in *Self-cleaning Materials and Surfaces*, ed. Walid Daoud, Woodhead, UK, 2013, ch. 7, pp. 205–224.
13 A. Bozzi, T. Yuranova and J. Kiwi, *J. Photochem. Photobiol., A*, 2005, **172**, 27.
14 A. Bozzi, T. Yuranova, I. Guasaquillo, D. Laub and J. Kiwi, *J. Photochem. Photobiol., A*, 2005, **174**, 156.

15 M. I. Mejia, J. M. Marin, G. Restrepo, C. Pulgarin, E. Mielczarski, J. Mielczarski, Y. Arroyo, J.-C. Lavanchy and J. Kiwi, *Appl. Catal., B*, 2009, **91**, 481.
16 M. I. Mejia, J. M. Marin, G. Restrepo, C. Pulgarin, E. Mielczarski, J. Mielczarski and J. Kiwi, *ACS Appl. Mater. Interfaces*, 2009, **1**, 2190.
17 X. Qiu, M. Miyaguchi, K. Sunada, M. Minoshima, M. Liu, Y. Lu, D. Li, Y. Shimodaira, Y. Hosogi, Y. Kuroda and K. Hashimoto, *ACS Nano*, 2012, **6**, 1609.
18 L. Zhang, R. Dillert, D. Bahnemann and M. Vormoor, *Energy Environ. Sci.*, 2012, **5**, 7491.
19 A. Mills, J. S. Wang, M. Crow, G. Taglioni and L. Novella, *J. Photochem. Photobiol., A*, 2007, **187**, 370.
20 N. Daels, M. Radoicic, M. Radetic, S. W. H. van Hulle and K. de Clerck, *Sep. Purif. Technol.*, 2014, **133**, 282.
21 T. Nardi, L. P. Canal, M. Hausmann, F. Dujonc, V. Michaud, J.-A. E. Månson and Y. Leterrier, *Prog. Org. Coat.*, 2015, **87**, 204.
22 T. Nardi, A. Karimi, Y. Leterrier and J.-A. E. Månson, *RSC Adv.*, 2014, **4**, 7246.
23 T. Nardi, Y. Leterrier and J.-A. E. Månson, *MRS Online Proc. Libr.*, 2014, **1685**, 1.
24 C. Ruales-Lonfat, N. Benitez, A. Sienkiewicz and C. Pulgarin, *Appl. Catal., B*, 2014, **160–161**, 286.
25 A.-H. Lu, W. Schmidt, N. Matoussevitch, H. Bonnemann, B. Spliethoff, B. Tesche, E. Bill, W. Kiefer and F. Schuth, *Angew. Chem., Int. Ed.*, 2004, **43**, 4303.
26 T. Nardi, M. Sangermano, Y. Leterrier, P. Allia, P. Tiberto and J.-A. E. Månson, *Polymer*, 2013, **54**, 4472.
27 A. K. Gupta and M. Gupta, *Biomaterials*, 2005, **26**, 3995.
28 B. Tian, T. Wang, R. Dong, S. Bao, F. Yang and J. Zhang, *Appl. Catal., B*, 2014, **147**, 22.
29 A. A. Bumb, P. L. Choyke, L. Fugger, A. Eggeman and D. Prabhakaran, *Nanotechnology*, 2008, **19**, 335601.
30 M. T. Buscaglia, L. Curecheriu, P. Postolache, L. Mitoseriu, A. C. Ianculescu, B. S. Vasile and P. Nanni, *Chem. Mater.*, 2010, **22**, 4740.
31 A. Bonnefond, E. Gonzalez, J.-M. Asua, J. Ramon Leiza, J. Kiwi, C. Pulgarin and S. Rtimi, *Colloids Surf., B*, 2015, **135**, 1.
32 S. Rtimi, O. Baghriche, C. Pulgarin, J.-C. Lavanchy and J. Kiwi, *Surf. Coat. Technol.*, 2013, **232**, 804.
33 H. Zhang, G. Chen and D. W. Bahnemann, *J. Mater. Chem.*, 2009, **19**, 5089.
34 J. Podporska-Carroll, E. Panaitescu, B. Quilty, L. L. Wang, L. Menon and S. C. Pillai, *Appl. Catal., B*, 2015, **176**, 70.
35 J. Fernandez, P. Maruthamuthu and J. Kiwi, *J. Photochem. Photobiol., A*, 2004, **161**, 185.